Research on Engineering Structures & Materials
www.jresm.org
Research Group

Research Article

Optimization of mechanical properties in multilayer multipass friction stir welding of dissimilar aluminum alloys

Chakrasali Chandrakumar [*,1, a], Irappa Sogalad [2,b], Akash Korgal [3,c], Madeva Nagaral [4,d]

[1]*Dept. of Mechanical Eng., Proudhadevaraya Institute of Technology, Hospet, Karnataka, India*
[2]*Dept. of Mechanical Eng., University BDT College of Engineering, Davanagere, Karnataka, India*
[3]*Dept. of Mechanical Eng., National Institute of Technology, Surathkal, Karnataka, India*
[4]*Aircraft Research and Design Centre, Hindustan Aeronautics Limited, Bangalore, Karnataka, India*

Article Info

Article History:

Received 02 Feb 2025
Accepted 19 July 2025

Keywords:

Multilayer-multipass-friction stir welding
ANOVA;
Friction stir welding joint;
Taguchi's DOE

Abstract

Friction stir welded butt/lap joints produced from different aluminum 6061-T651 and 7075-T651 alloys will be examined to investigate the effect of various process parameters on mechanical properties. The present work investigated the potential application of the multilayer-multipass friction stir welding (MM-FSW) process to restructure the fabrication of thick-section components using dissimilar aluminum alloy materials, offering a new avenue for industries that require durable and reliable welds. In this study, aluminum 6061-T651 alloy is considered as the base plate with a thickness of 10 mm. The assembly involved stacking two layers and five passes of 3 mm-thick aluminum 7075-T651 alloy plates onto pre-machined stepped grooves in the AA6061-T651 base plate, followed by friction stir welding to create a 10 mm-thick plate. This study investigates the influence of multiple process variables, including rotation speed, traverse speed, and tool pin geometry, on the mechanical properties of the associated butt/lap joint configuration in MM-FS welded dissimilar AA6061-T651 and AA7075-T651 alloys employing Taguchi methods. The optimum tensile strength of 202.65 MPa was obtained at rotational, travel, and tool pin profiles of 1100 rpm, 20 mm/min, and a threadless taper tool pin geometry, respectively, according to the signal-to-noise (S/N) ratio analysis. Additionally, the ANOVA analysis discovered that the rotational speed, tool pin shape, and traverse speed contribute 50.57%, 13.98%, and 35.01%, respectively.

1. Introduction

Friction Stir Welding (FSW) is a solid-state joining method that fuses materials without reaching their melting points. It generates friction between the tool and probe, causing heat to plasticize the metal at the joint. This flexible substance allows the rotating pin to engage and blend thermoplastic materials, resulting in defect-free, robust adhesion. FSW is ideal for applications requiring exceptional mechanical strength, such as aerospace, automotive, and shipbuilding [1,2]. The Welding Institute (TWI)introduced a method in 1991, known for its energy efficiency and environmental consciousness, reducing fumes, arc flashes, spattering, distortions, and residual stresses compared to fusion welding techniques [3]. B. Thompson et al. [4] optimized tool profiles for welding specific alloys, resulting in tools capable of sustaining operations for 500 inches without failures. AA5059 and AA2139 exhibited exceptional performance, while AA2139 reached 90% of the performance level in monolithic plate configurations. M. Imam et al. [5] developed a preheating method and composite backing plate strategy to enhance joint properties in FSW for

*Corresponding author: chakrasali@pdit.ac.in
[a]orcid.org/0009-0004-0618-6915; [b]orcid.org/0000-0002-4475-3579; [c]orcid.org/0000-0003-0273-7746; [d]orcid.org/0000-0002-6237-3983
DOI: http://dx.doi.org/10.17515/resm2025-643me0202rs

thicker sections, reducing forge axis loads, power consumption, and tool wear. D. A. Kumar et al. [6] identified trapezoidal pin geometry tools as suitable for defect-free welding, predicting adequate tensile strength and ductility at high tool rotational speeds and low welding speeds. Z. Liang et al. [7] investigated the friction stir welding of 6082 aluminum alloy in a 42 mm thick plate, revealing a kissing bond defect that did not affect the ultimate tensile strength. P. A. Colegrove et al. [8] optimized welding thickness for 20 mm-thick 7449 aluminum alloy for aerospace applications, demonstrating the significance of tool rotational speed for successful weld execution. J. P. Martin [9] developed innovative techniques for friction stir welding of thick-section aluminum alloys to reduce production cycle time, distortion, and part handling. Their research indicated that enhancing weld quality can provide consistent and uniform heat input, extend tool lifespan, and lower tooling costs. Y. C. Lim [10] studied the mechanical properties and microstructural characteristics of a multi-layered, multipass friction stir weld applied to ASTM A572 Grade 50 low-alloy steel. They found that the tensile strength closely mirrored the original base metal, and there were elevated hardness levels in the Mixing Zone and Heat-Affected Zone. Fractures were predominantly found within the base material. K. Wang et al. [11] found that an extended process window for defect-free multi-layer connections by micro friction stir welding was ideal, with grain modifications and hardness detected in the weld zone. M. Tariq [12] examined the FSW method for the butt joint of Al-1350 bi-layered laminated sheets, finding that FSW parameters significantly impact defect formation, material mixing, and particle strengthening dissolution. M. Sajed et al. [13] invented a new solid-state welding method called "multi-layer friction stir plug welding" for thick aluminum plates, achieving a joint strength of 124 MPa. D. Gera et al. [14] used the refill friction stir spot welding technique to join aluminum 2024-T3 alloy sheets to multi-layered aluminum foils, achieving flawless welds with substantial lap shear strength. Dynamic recrystallization refined the 2024 Al alloy in the shoulder replenishment zone, while refill FSSW generated minimal contact resistance. J. Taendl et al. [15] improved the mechanical characteristics and microstructure of 15-layer friction stir butt welded steel, resulting in flawless welds with a tensile strength of 1240 MPa, a fracture elongation of 13%, and a joint efficiency of 90%. Heat treatment restored the hardness of martensitic layers, improving tensile properties to 1310 MPa with 95% joint efficiency and 22% fracture elongation. A. Das et al. [16] explored the impact of overlapping percentages on joining two layers of AA6061-T6 alloy using the multi-track FSAM approach, resulting in extensive plasticized material mixing and an impenetrable microstructure. L. Chen et al. [17] used the additive friction stir deposition technique to fabricate multi-layer aluminum 6061 alloy components, demonstrating that heat treatment significantly impacted the microstructure and electrochemical behavior related to corrosion. A. Hassan et al. [18] found that the threaded taper pin tool produced impeccable laminates at 500 rpm and 1200 rpm, with enhanced microhardness linked to a grain size range of 0.96 to 1.47 μm. This led to a 95.61% reduction in grain size compared to the base material. An increase in welding speed and building height was associated with improved microhardness. M. Orłowska et al. [19] found that microhardness increased in a similar weld from coarse-grained aluminum within the stir zone due to a decrease in average grain size. Y. Yang et al. [20] investigated the improvement of mechanical properties, corrosion, and tribological performances of an AA5083/316 stainless steel surface composite through friction stirs processing. Results show that multi-pass FSP refines grain, improves reinforcement scattering, enhances mechanical and wear properties, and improves corrosion resistance. Laska et al. [21, 22] conducted several studies on friction stir welding (FSW) of aluminum alloys, focusing on how welding parameters, tool rotational speed, and tool geometry affect the mechanical, chemical, and microstructural properties of joints. Their research on AA6082 and AA5083/AA6060 joints indicated that optimizing parameters like tool speed and geometry significantly improves strength, corrosion resistance, and material flow. Aleksandra et al. [23, 24] examined the role of residual stresses and dislocation density in influencing deformation characteristics. Overall, their work offers key insights into enhancing weld quality through careful control of FSW parameters and tool design. Cole et al. [25] established the nominal friction stir welding process parameters for joining aluminum alloys 6061-T6 and 7075-T6 and improved joint quality through programmed tool offsets. They found that weld tool offsets increase joint strength, facilitated by lower average weld temperatures with increasing AA7075 stirring. Seshu Kumar et al. [26] analyzed the FSW process on aluminum 7075 and 6061 alloys using the Taguchi design approach, finding that the tool's

rotating speed and angle of inclination are more influential characteristics than the axial force exerted on the welded joints. As the tool's rotational speed escalates, the effective thrust strength also grows, with the effective IS rising to 900 rpm and the effective HV reaching 2.5 kN. Ghiasvand et al. [27] examined underwater dissimilar friction stir welding of AA6061 and AA7075 aluminum alloys to mitigate hardness reduction in microstructural regions. They found that the AA7075 side experienced the same repair mechanisms as traditional friction stir welding, but the AA6061 side had finer grains. Ghiasvand et al. [28] and Chen et al. [29] conducted numerical simulations using ABAQUS software to analyze the impact of tool-positioning factors on maximum temperature in a dissimilar friction stir welding (FSW) joint of AA6061-T6 and AA7075-T6 aluminum alloys. They found that plunge depth, tilt angle, and tool offset were the most significant factors affecting the maximum process temperature and Ultimate Tensile Strength of the joints. Parasuraman et al. [30] evaluated the fracture toughness of welded joints using FSW AA7075-T651 specimens. Results showed superior tensile strength and fracture toughness, which were attributed to the evolution of finer grains in the SZ due to the stirring action of the FSW tool. Concerns arise from inadequate stirring caused by heat loss to the backup plate material. To address the constraints above, an endeavor has been undertaken to investigate the feasibility of employing a multi-layer multipass friction stir welding (MM-FSW) approach for thick aluminum structures. This approach, previously demonstrated in the author's recent work concerning steel by Y. C. Lim et al. [31][32, 33], is now applied to fabricating a multi-layer structure using aluminum alloy.

In the previous literature, many authors focused on different techniques to weld thick aluminum alloy plates, such as the double-sided welding method, layer-by-layer stoking method, using a single-tool geometry, bobbin tool type, and limited process windows. However, the present investigation, there is a specialty in the multi-layer multipass friction stir welding (MM-FSW) technique, is to address the difficulties associated with welding of any thickness of thick aluminum alloy as compared to other methods. Another advantage of this technique is that it can be used to repair cracks and voids in thick aluminum plates. The primary objective of the present research is to develop a multi-layer structure via the friction stir welding technique, wherein two layers of AA7075-T651 metal are stacked upon a pre-machined AA6061-T651 alloy base. The effects of tool rotation speed, welding speed, and tool pin profile on ultimate tensile strength were studied. This work extends previous research that examined the primary factors affecting the improvement of ultimate tensile strength (UTS) in AA6061-T651 and AA7075-T651 joints produced by MM-FSW. The Taguchi Design of Experiments method, utilizing an L_9 Orthogonal Array, was employed to identify the optimal process variables, followed by an ANOVA analysis to estimate the contribution % of all parameters to tensile strength.

2. Experimental Procedure

2.1. Material Selection

In this ongoing investigation, the 10mm thickness of AA6061-T651 alloy is chosen as a base metal, and the AA7075-T651 alloy of 3mm thickness is considered for a supplementary stacking layer. AA 6061 alloys' primary strengthening precipitated phase is Mg_2Si, while Al_2CuMg and Cr-containing dispersoids contribute to age hardening, copper presence, and grain growth prevention during heat treatment. Whereas, the strength of the AA7075 alloy is primarily due to the production of MgZn2 during the aging process. The Al_2CuMg (S-phase) enhances the alloy's hardness and strength. Fe-containing Al_7Cu_2Fe and Al_7Cr precipitates alter mechanical characteristics and improve toughness and fatigue resistance [32, 33]. Joints between dissimilar materials of 6061 T6 and 7075-T6 by the MM-FSW process offer high strength and desirable quality welded joints by minimizing residual stresses and distortions, which are common in fusion welding. The welded components are ideal for various industries, including aerospace, automotive, marine, railway, and defense. They offer outstanding mechanical properties, corrosion resistance, and durability, making them suitable for aircraft fuselage panels, wing structures, chassis components, crash structures, shipbuilding, offshore structures, armor plating, and military vehicles [34]. The chemical constituents and mechanical characteristics of both AA6061-T651 and AA7075-T651 materials, respectively, are detailed in Tables 1 and 2. Applying energy dispersive X-ray

spectroscopy coupled with scanning electron microscopy, the chemical nature of the AA6061-T651 and AA7075-T651 has been examined (SEM-EDS).

Table 1. Base metal composition

Material	Dimensions									
	Al	Cr	Cu	Fe	Mg	Mn	Si	Ti	Zn	Other
AA6061-T651	98.6	0.35	0.40	0.70	1.2	0.15	0.80	0.15	0.25	0.05
AA7075-T651	91.4	0.28	2.0	0.50	2.9	0.30	0.40	0.20	6.1	0.05

Table 2. Mechanical characteristics of AA6061-T651 and AA7075-T651 alloy base materials

Property	AA6061-T651	AA7075-T651
Ultimate Tensile Strength	310.25 MPa	545.89 MPa
Yield Strength	275 MPa	503 MPa
Hardness of Material	95 Brinell	150 Brinell
Modulus of Elasticity	68.9 GPa	71.7 GPa

2.2. Tool Geometry

Our study explores using three distinct pin profiles during aluminum alloys' friction stir welding (FSW). This exploration aims to identify the most suitable tool type to facilitate defect-free welding while accommodating various process parameters. The selected tool has a 6mm pin diameter and an 18mm diameter shoulder with a flat and smooth surface design. An M6 thread tool pin is a metric tool with a 6 mm nominal diameter and a pitch of 1.0 mm, and is utilized in the current MM-Friction Stir Welding to improve material flow and promote bonding. M6 thread tools are suitable for welding thinner materials because the thread size can influence the material stirred and heat generation during the welding process. This design produces frictional heat and applies downward pressure without rapidly stirring the material. Specifically, the three tool profiles employed are as follows:

- a) A straight-pin tool with threads
- b) A tapered pin tool with threaded
- c) A tapered pin tool without threading

These tool variations, visually represented in Fig. 1, are an experimental approach to achieving optimal welding outcomes. The tool's material composition is high-speed H13 tool steel, deliberately chosen for its capacity to withstand the demanding conditions inherent to the welding procedure. In the current study, the clockwise direction of spindle rotation is preferred in Friction Stir Welding (FSW) when viewed from above because this direction of rotation ensures optimal material flow, effective heat generation, and better overall weld quality [35] as seen in Fig. 4, welded plates. The detailed specifications of the tool can be found in Table 3.

Table 3. Geometry of tools specification

Tool Geometry	Tool Pin Geometry	Shoulder Diameter	Pin Diameter		Length of Pin
			Major	Minor	
T1	Straight pin with threads	18 mm	6 mm	6 mm	3.4 mm
T2	Tapered pin with threads	18 mm	6 mm	3 mm	3.4 mm
T3	Tapered pin without threads	18 mm	6 mm	3 mm	3.4 mm

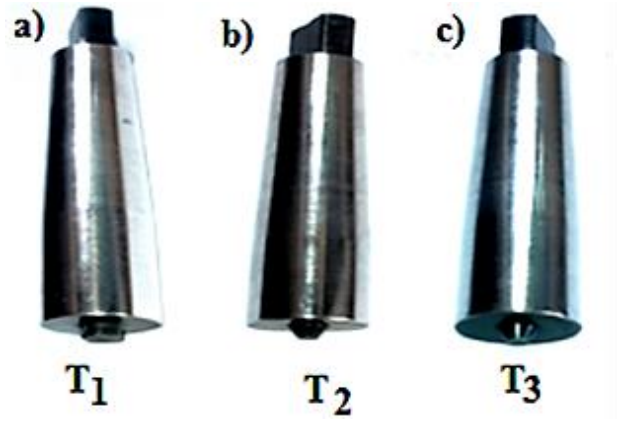

Fig. 1. Tool pin geometries used for the welding process: (a) Straight threaded pin, (b) Threaded tapered pin, (c) Tapered Threadless pin

2.3. Experimental Procedure

The Multi-layer Multipass Friction Stir Welding (MM-FSW) process is illustrated in Fig. 2. Illustrated in Fig. 3 are the successive stages of the Multi-layer Multipass Friction Stir Welding (MM-FSW) process. Before welding, a steel plate is placed on the workbench of the FSW machine as a "Backing Plate". Because it can endure the substantial stresses exerted during FSW and efficiently distributes heat, hence reducing excessive thermal accumulation at the weld contact.

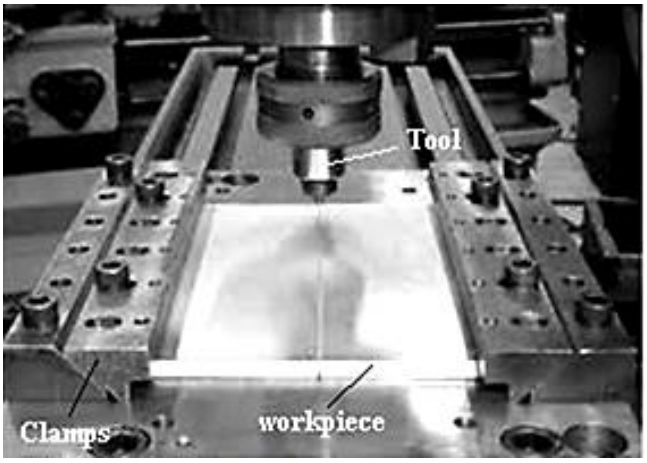

Fig. 2. Friction Stir Welding Process

Initially, the base material was chosen as an AA6061-T651 alloy plate measuring 120mm x 260mm x 10mm. This base plate underwent machining on a Vertical Milling Machine fabricated by Kirloskar to create a stepped assembly of the desired dimensions, a configuration essential to accommodate the MM-FSW procedure, as depicted in Fig. 3(A).

Firstly, the two pieces of machined plate of size 120x130x10 mm are brought into contact with each other and then friction stir welded together with the help of a 3.5 mm depth welding tool pin and employing a standard butt joint configuration at point 1 on the bottom or root, as illustrated in Fig. 3(B). The plunge depth of the 3.4 mm tool pin was used to join the AA6061-T651 alloy base plates with a constant 0° tilt angle using a CNC friction stir processing System manufactured by Interface Design Associates Pvt. Ltd.

In the next step, the first plate, a AA7075-T651 alloy with size of 120mm x 76.4mm x 3mm plate was inserted on above the welded assembly as shown in Fig. 3 (C) for the subsequent creation of a multi-layered structure with a welding depth of 3.4mm on both sides i.e. is one at locations 2 and other at location 3 to create the butt / lap-type configuration joints as shown in Fig. 5 using a friction stir welding machine.

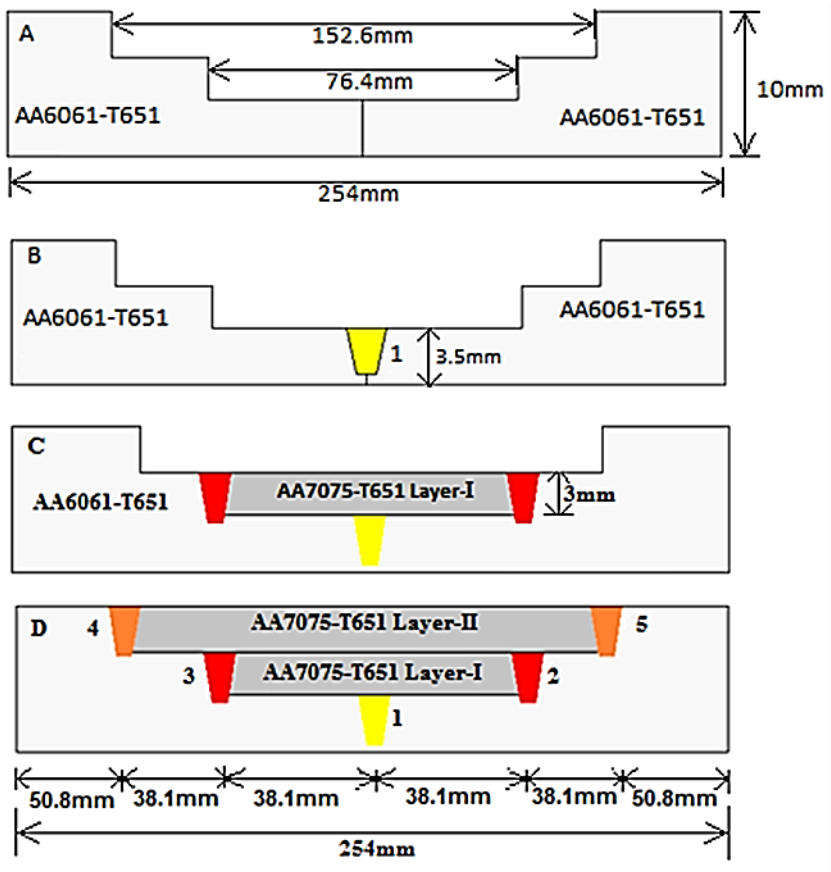

Fig. 3. Schematic diagram of MM-FSW process, (A) Showing the cross-sectional view of pre-machined AA6061-T651 material for MM-FSW, (B) A butt weld configuration for the bottom layer, (C) FSW and insertion the first weld plate on top of the root weld, and (D) Situation of the second weld plate on top of the first welded plate and the finished weld structure followed by FSW

Lastly, the second AA7075-T651 alloy plate, measuring 120mm x 152.4mm x 3mm, was positioned on top of the previously inserted AA7075-T651 alloy welded plate. Similar to the previous step, this plate was joined at points 4 and 5 with a lap/butt joint configuration using friction stir welding, as shown in Fig. 3(D). A key aspect of this process is that only one pass was performed at each junction of the two plates. This results in a total of five passes for the entire process, indicated by the numbers 1-5 in Fig. 4 (A)-(D). Notably, the welded geometry combines butt and lap joints, arising from the addition of extra metal layers into the pre-machined workpiece, thus referred to as a 'butt/lap' joint, as illustrated in Fig. 5. The plunge depth employed in this study was 3.4 mm, with the tool inclination angle set at 0°. Welding of the 10 mm-thick samples was carried out using a vertical CNC welding machine located in NITK Surathkal, which features a high-power spindle with a 22-kW capacity, a 4-axis digital numerical control system, support for G and M Code, a frame capacity of 50 kN, and maximum stroke lengths of 500 mm along the X- and Y-axes and 300 mm along the Z-axis, along with a unique clamping mechanism and temperature measurement implementation inside the working zone.

To prevent overlap with the previous layer, a transverse offset of 38.1 mm was applied on both sides for each successive layer. The primary objective of selecting five passes and two layers in the MM-FSW process is to address the numerous challenges in dissimilar alloys welding, such as those encountered with AA6061 and AA7075 alloys. A single pass may not adequately penetrate the stir material across the weld line of a thick aluminum plate. Therefore, five passes were necessary to ensure sufficient material flow and defect closure while balancing process time and energy consumption. Likewise, two layers were chosen to achieve the desired joint thickness without causing excessive thermal buildup, which could negatively impact the mechanical properties.

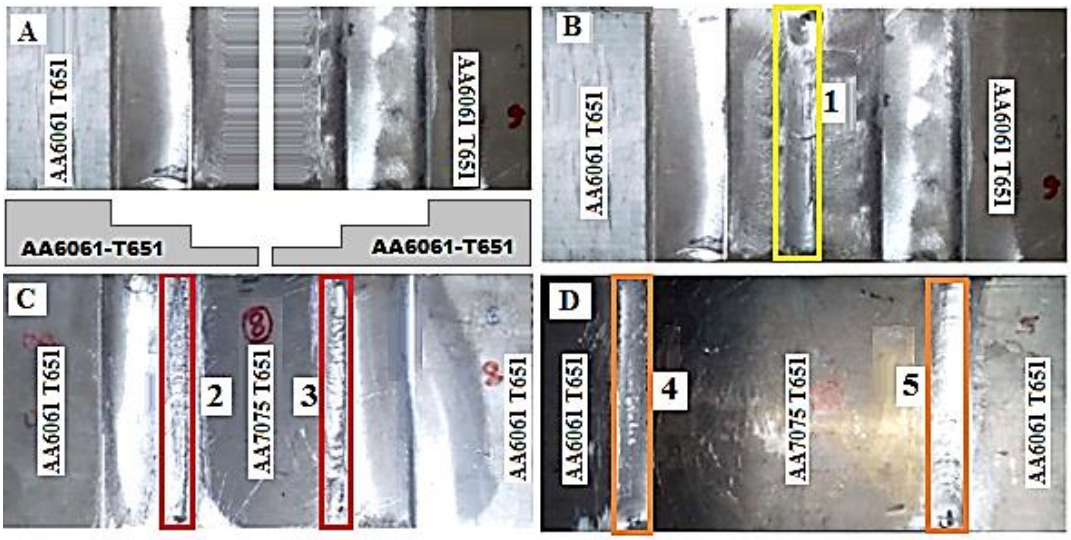

Fig. 4. Steps followed in MM-FSW, (A) Stepped section of base AA6061-T651 Plate, (B) First butt-joint welded region at point 1. (C) AA7075-T651 alloy plate was inserted above the welded base plate and welded at region 2 and 3, (D) Final another AA7075-T651 plate insertion over the first 7075-T651 welded plate and welded at points 4 and 5

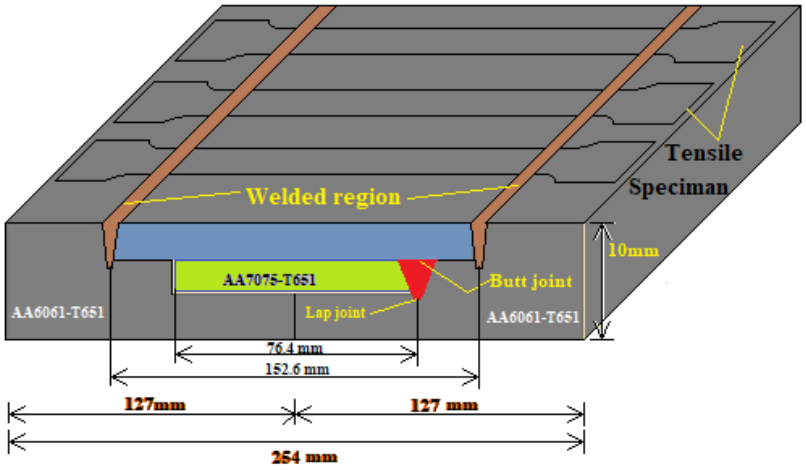

Fig. 5. Representation of both butt/lap joint configuration

2.4. Preparation of Specimen

For this investigation, commercially available aluminum alloys 6061-T651 and 7075-T651 were procured as plates, conforming to the required dimensions. All edges of these plates underwent shearing, while the face surfaces were meticulously milled on a vertical milling machine. This process ensured a high-quality surface finish and verified perpendicularity. Before welding, the edges were further treated with emery paper to eliminate any residual dirt and debris.

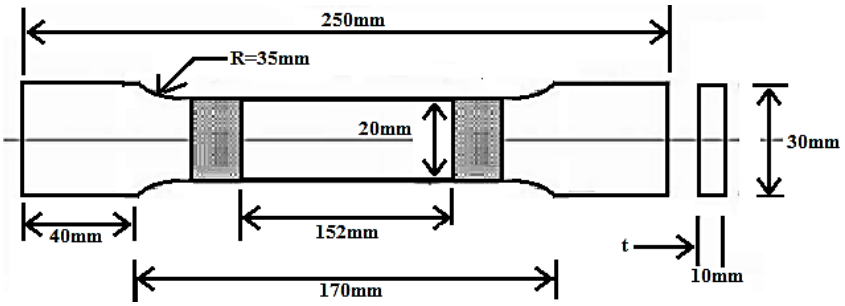

Fig. 6. Dimension of a tensile test specimen

According to ASTM E8-04 standards [36], two sets of nine tensile test specimens were carefully prepared using J. K. Machine wire-cut EDM and the same dimensions as considered in Reference [10]. The tensile tests are conducted at room temperature using a UTM. The tensile strength test mean values are considered for the analysis. The detailed dimensions of the tensile test specimen are illustrated in Fig. 6.

2.5. Taguchi Method

This study refined the parameters of Friction Stir Welding (FSW) through the application of the Taguchi design of experiments, utilizing an L_9 orthogonal array. This arrangement featured three columns and three rows. The investigation focused on examining the effects of AA6061-T651 and AA7075-T651 alloys under different process parameters, such as the speed of rotation (S), transverse speed (F), and tool pin type (T).

Employing the Taguchi method, the experimental data underwent analysis by assessing the S/N ratio (Signal-to-noise) for each process parameter level. Irrespective of the specific quality characteristic being considered, a higher signal-to-noise ratio corresponds to a more favorable quality attribute [37, 38]. Consequently, the optimal process parameter level is identified as yielding the highest S/N ratio. As shown in Fig. 7, nine tensile tests were performed on AA6061-T651 and AA7075-T651 materials joints prepared from the MM-friction stir welding technique. The design of the process parameters [39] adhered to the principles of the L_9 (3^3) orthogonal array, which accommodates three levels and three factors as considered in reference [26], shown in Table 4. The fracture specimens from the tensile test were subjected to Scanning Electron Microscopy (SEM) to analyze the fracture mechanism.

Fig. 7. Tensile experiment tested specimens

Table 4. presents three process factors and levels in detail

Process Parameters	Level 1	Level 2	Level 3
Rotational Speed (RS) in RPM	700	900	1100
Travers speed (TS) in mm/min	20	30	40
Tool Pin Geometry (TG)*	T1	T2	T3

* T1= Straight Threaded Pin, T2= Taper threaded Pin, T3=Taper Threadless Pin Geometry

3. Findings and Analysis

3.1. Mechanical Properties of the Welded Alloy

The Microstructure of the AA6061-T651 and AA7075-T651 is shown in Fig. 8. In the investigation of the microstructure and Energy Dispersive X-ray Spectroscopy (EDS) of aluminum alloys

AA6061-T651 and AA7075-T651, distinct characteristics and elemental compositions were observed, shedding light on their structural properties and suitability for various applications.

AA6061-T651, characterized by the presence of magnesium (Mg) and silicon (Si), Fig. 8(a), represents an alloy renowned for its excellent weldability and corrosion resistance. Magnesium imparts strength to the alloy, while silicon enhances strength and heat resistance. Microstructural analysis of AA6061-T651 reveals a precipitation hardening mechanism, where the formation of Mg_2Si precipitates contributes significantly to its mechanical properties. The EDS analysis further validates the alloy's composition by confirming the presence of essential elements like Mg and Si.

In the case of AA7075-T651, the alloy showcases a distinctive composition comprising zinc (Zn), copper (Cu), and magnesium (Mg), Fig. 8(b). Zinc contributes to high strength and corrosion resistance, while copper enhances strength through solid solution strengthening and precipitation hardening. Like AA6061, magnesium in AA7075 provides additional strength, and the microstructural analysis reveals the formation of $MgZn_2$ and Mg_2Cu precipitates during precipitation hardening. The EDS examination reaffirms the alloy's composition by confirming the presence of zinc, copper, and magnesium.

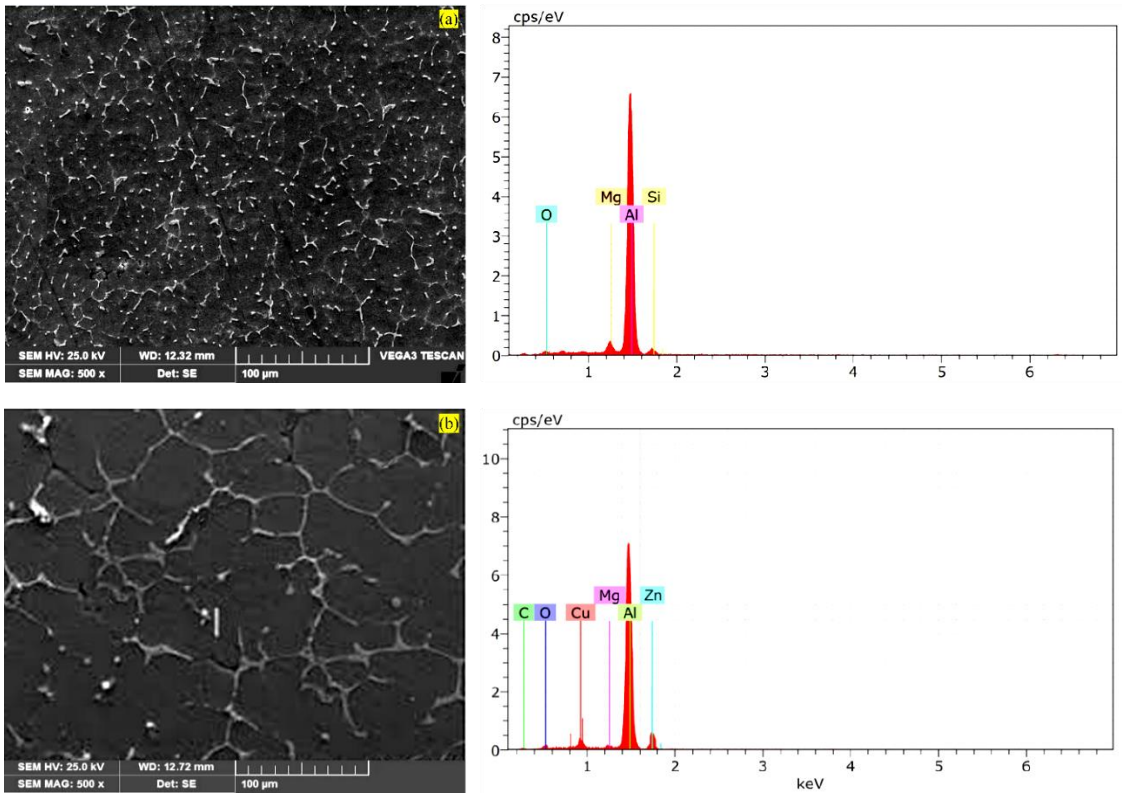

Fig. 8. Microstructure and EDS of (a) AA6061-T651, (b)AA7075-T651 tested Specimens

This study involved conducting mechanical tests with a Universal Testing Machine to determine the ultimate tensile strength of nine different tensile specimens. The results, showcasing the values of final tensile strength, are summarized in Table 5. It is observed that the peak ultimate tensile strength value, attaining 202.65 MPa, has been accomplished at a rotational speed of 1100 rpm and a traverse speed of 20 mm/min, employing a threadless taper pin tool profile. At these optimized parameters, because of the low traverse speed and high rotational speed of the tool, produces sufficient amount of heat is generated and proper mixing of material takes place. This result is comparable to the findings of Rodriguez et al. [40], who reported a peak UTS of 192.6 MPa for dissimilar AA6061-AA7050 welds processed at 410 rpm. However, our approach, employing a multilayer multipass technique, resulted in more uniform mechanical properties and reduced variability across layers, which is not addressed in the single-pass configuration reported in the reference.

Table 5. Results of tensile strength properties

Sl. No	RS (RPM)	TS (mm/min)	TG	UTS (MPa)
1	700	20	T1	177.000
2	700	30	T2	169.900
3	700	40	T3	194.466
4	900	20	T2	172.700
5	900	30	T3	188.023
6	900	40	T1	184.994
7	1100	20	T3	202.650
8	1100	30	T1	192.050
9	1100	40	T2	197.040

3.2. ANOVA Results

In the present study, the statistical technique known as ANOVA has been employed to determine the influence of various process factors on the strength of welded joints [41]. Analyzing F-values reveals that the most significant factors affecting joint strength are the speed of rotation, speed of welding, and geometry of the tool pin, in that sequence [42]. The concept of percentage contribution (P) is integral to understanding the extent of influence each parameter has on the observed changes in experimental outcomes. A higher percentage contribution indicates a tremendous potential for impacting the welding process's overall performance. The correlation coefficient R^2 value obtained was 0.9966, as revealed in Table 7. It can be concluded that the rotational speed (RS) is the most significant factor affecting the tensile strength of the welded joint, as indicated by the analysis of variance, accounting for approximately 50.57% of the total variance. In comparison, the speed of rotation (TS) contributes 13.98%, while tool pin geometry (TG) contributes 35.10% to the overall strength of the welded joint, as shown in Table 6. The pooled error associated with the ANOVA is ~1.74 %. ANOVA clearly shows that, as rotational speed increases, sufficient heat is produced during the welding process, resulting it creates a defect-free weld with a higher value of tensile strength.

Table 6. Process parameters contributions from ANOVA

Source	DF	Adj SS	% of contribution	Adj MS	F-Value	P-Value
A-RS	2	519.40	50.57 %	259.699	149.24	0.007
B-TS	2	143.62	13.98%	71.809	41.27	0.024
C-TG	2	360.50	35.10%	180.252	103.59	0.010
Error	2	3.48	0.35%	1.740		
Total	8	1027.00	100%			

DF: Degrees of Freedom, Adj SS: Adjusted Sum of Squares, Adj MS: Adjusted Mean Squares

Table 7 The basic Taguchi L_9 (3^3) orthogonal array and experimental values of equivalent stress (mean) and S/N ratio. The fracture specimens from the tensile test were subjected to Scanning Electron Microscopy (SEM) to analyze the fracture mechanism. This process ensured a high-quality surface finish and verified perpendicularity. Before welding, the edges were further treated with emery paper to eliminate any residual dirt and debris.

In Table 7, the F-value indicates the relative impact of each process parameter by comparing the variance caused by that factor to the residual variance (error). A higher F-value signifies that the factor has a more substantial effect on the response variable. It can be concluded that the F-value of rotational speed and tool pin geometry are higher values, which means both parameters are responsible for increasing the strength of the material. Whereas the P-value of all the process parameters is less than 0.05 and indicating that the factor's effect is statistically significant at a 95% confidence level.

Table 7. The basic Taguchi L_9 (3^3) orthogonal array and experimental values of equivalent stress (mean) and S/N ratio

Sl. No	RS (RPM)	TS (mm/min)	TG	UTS (MPa)	SNRA1	MEAN1
1	700	20	T1	177.000	44.9595	177.000
2	700	30	T2	169.900	44.6039	169.900
3	700	40	T3	194.466	45.7769	194.466
4	900	20	T2	172.700	44.7458	172.700
5	900	30	T3	188.023	45.4842	188.023
6	900	40	T1	184.994	45.3432	184.994
7	1100	20	T3	202.650	46.1349	202.650
8	1100	30	T1	192.050	45.6683	192.050
9	1100	40	T2	197.040	45.8911	197.040

3.3. Main Effect Plot for S/N Ratio

This analysis's primary focus revolved around investigating tensile strength, which is the critical parameter for attaining a well-constructed joint. The approach adopted in this study involved utilizing the "larger the better" signal-to-noise (S/N) ratio model, which enabled the identification of optimal parameters. This choice ensured that the resultant strength values were more practical and conducive to effective comparisons. A response table encompassing means and S/N ratio was formulated to compile comprehensive results based on the experimental data. This tabulated information is presented in Tables 8 and 9, offering insights into the analysis outcomes.

Table 8. Mean response

Level	A-RS (RPM)	B-TS (mm/min)	C-TG
1	180.5	184.1	184.7
2	181.9	183.3	179.9
3	197.2	192.2	195.0
Delta	16.8	8.8	15.2
Rank	1	3	2

Table 9. Response of signal to noise ratios (largest is better)

Sl. No	RS (RPM)	TS (mm/min)	TG
1	45.11	45.28	45.32
2	45.19	45.25	45.08
3	45.90	45.67	45.80
Delta	0.78	0.42	0.72
Rank	1	3	2

The study's primary objective was to achieve the maximum tensile strength for the specified alloys in the joints. Consequently, pursuing the highest S/N ratio was a pivotal element, as it signifies the optimum level of process parameters, which holds particularly true for quality characteristics adhering to the "higher the better" principle. The specific formula used for calculating the Signal-to-Noise (S/N) ratio is based on the “Larger-the-better” criterion, which is appropriate for maximizing responses of tensile strength. The formula is:

$$\frac{S}{N} = -10.log_{10}(\frac{1}{n}\sum_{i=1}^{n}\frac{1}{y_i^2}) \quad (1)$$

Where, n: number of observations, y_i: observed response value of tensile strength

The factors were ranked according to their Delta value, the difference between the highest and lowest average response across levels. A higher Delta indicates a stronger influence on the response variable. A (Rotational Speed, RS) exhibited the highest Delta (16.8), followed by C (Tool Geometry, TG) with a Delta of 15.2, and B (Traverse Speed, TS) with 8.8. The optimal Level Combination based on the highest mean response is A3–B3–C3.

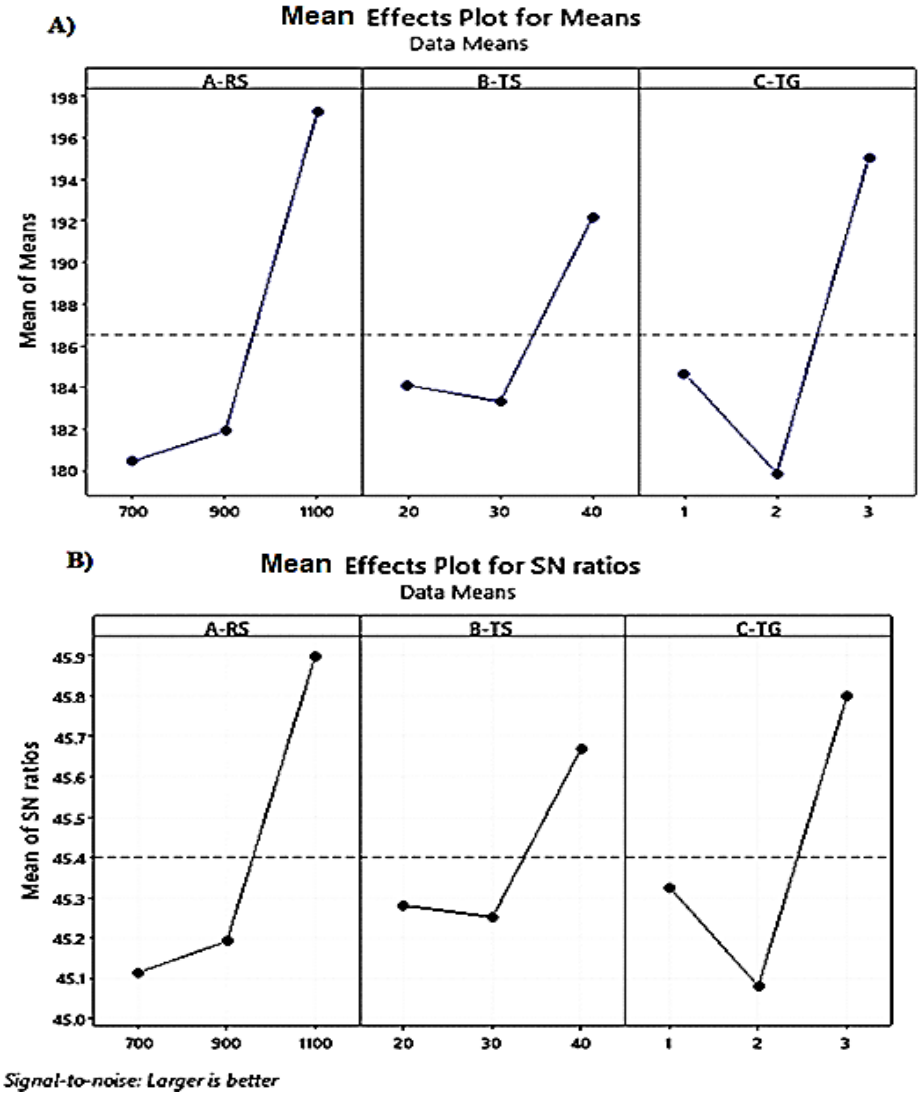

Fig. 9. Mean effects plots for Ultimate tensile strength (A) Means, (B) S/N ratios

Fig. 9 (A)-(B) illustrates the mean effect plots showcasing the Mean and S/N ratios. These plots visually represent the response of S/N ratio values concerning welding speed, feed rate, and tool type. A discernible pattern emerges: the mean and S/N ratio values ascend as the speed increases. However, a departure from this trend is observed when the rotational speed exceeds a certain point, resulting in a decrease in the S/N ratio. This is attributed to the inverse relationship between increased speed and the strength of bonding, where heightened speed can compromise the bond's strength. The contour plot highlights a positive correlation among three critical factors in our study: the speed of rotation, welding speed, and tool pin geometry, as well as their impact on the material's strength, as illustrated in Fig. 10. These contour plots demonstrate how variations in parameters affect the material's joint strength characteristics.

Upon closer examination of the plot, a distinct trend emerges: an increase in material strength as the rotational traverse speed is changed about the tool pin geometry. As observed in the figure, the contour lines form a series of interconnected curves and regions, highlighting that up to the 700-900 rpm speed, 20-30 mm/min welding speed, and for all three tool pin geometries, the strength of the material tend to exhibit low tensile strengths because when tool rotated at slower rates

causes the insufficient stirring action similar experimental results was observed in reference obtained by Das et al. [43]. However, when we increase the speed and feed to 1100 rpm and 40 mm/minute, respectively, the joint strength is enhanced because when the speed increases, high heat is generated; meanwhile, acceptable gains are produced along with proper mixing.

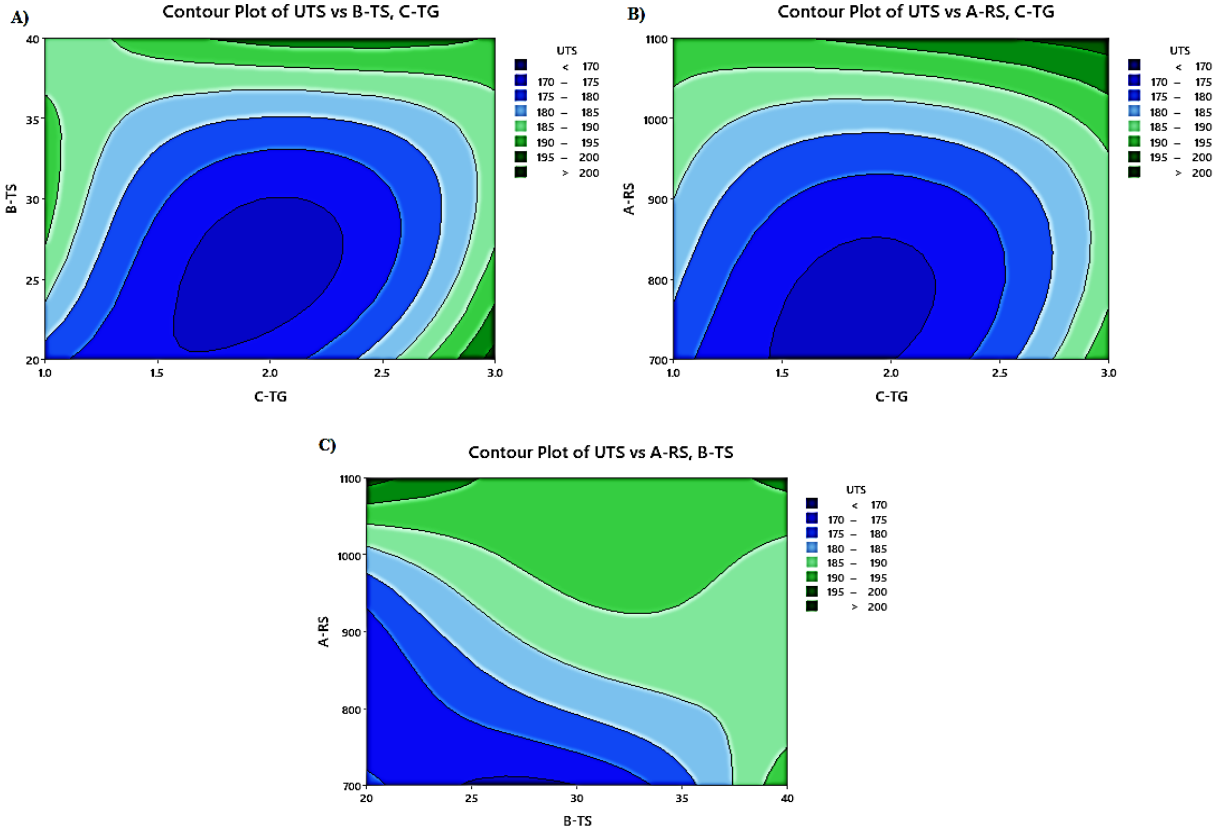

Fig. 10. Contour plots of UTS v/s A) TS&TG, B) RS&TG, and C) RS&TS

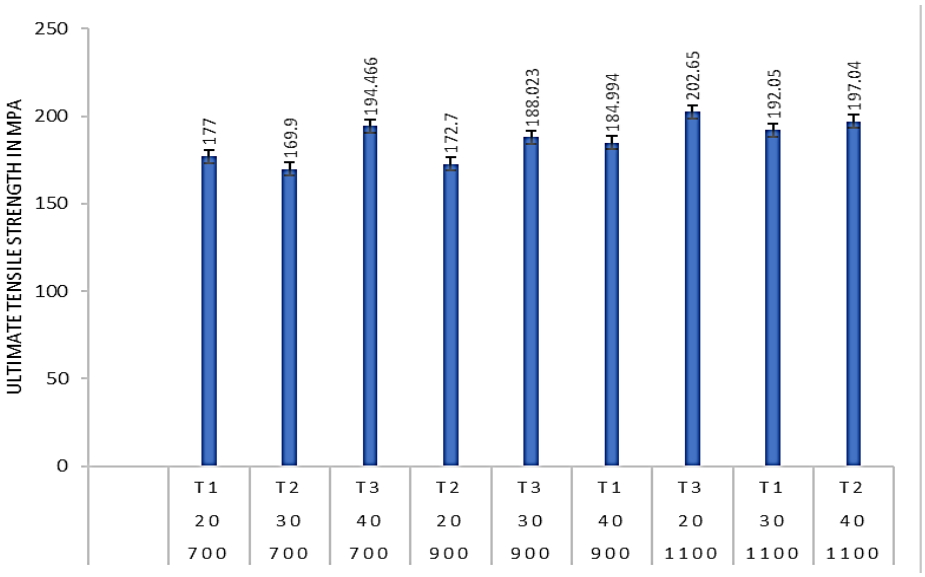

Fig. 11. Contour plot error bar chart

Fig. 11 represents the error bar chart of the ultimate tensile strength of dissimilar aluminum alloys. The main challenge in the case of MM-FSW is that it combines lab joint and butt joint configurations by adding a metal plate to stack the subsequent layer, known as the "butt/lap" nomenclature. This butt/lap joint design results in the interface fault known as a "hooking defect". This defect frequently arises at a lap joint due to the upward movement of the metal at the horizontal interface

when the tool engages with the lower layer. The challenge was addressed by positioning the tool's advancing side on the lap interface side of the corner joint, effectively minimizing hooking as seen in reference [10]. In conclusion, the threadless taper pin geometry operating at 1100 rpm demonstrates the greatest material tensile strength because the weld zone is free of defects, as highlighted in the reference [44]. Fig. 12 illustrates the tensile strength comparison among the 6061-T6 workpiece, the 7075-T651 workpiece, and the MM-FSWed dissimilar AA6061-T651 and AA7075-T651 workpieces. The tensile strength measurements of the MM-FSWed workpiece indicate a lower value of approximately 53.09% compared to the 6061-T6 workpiece and 169.37% compared to the 7075-T651 workpiece.

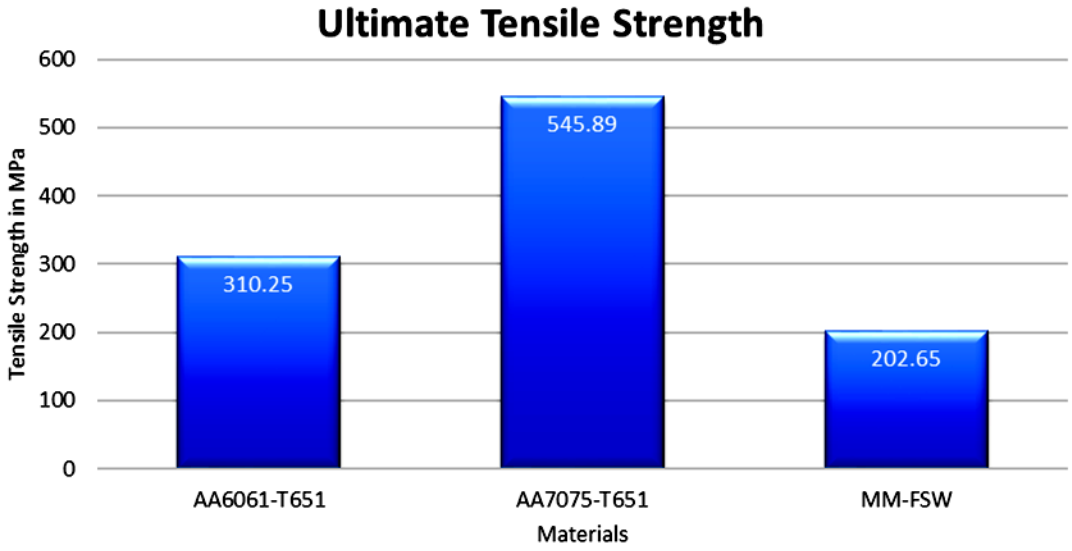

Fig. 12. Comparative results of ultimate tensile strength properties

3.4. Fracture Surface Analysis

The analysis of fracture surfaces in specimens tested under tensile forces, as shown in Fig. 13, features scanning electron microscopy (SEM) micrographs of weldments with Al6061 and Al7075 tensile specimens. Notably, the pores on the fracture surface of the Al6061 weld metal were larger than those on the surface of the material. Both specimens showed a dimpled feature, indicating ductile failure at room temperature. In Fig. 13 (a), the Al6061-T651 weldment displayed fine dimples, suggesting a highly plastic deformation characteristic, in contrast to the Al7075-T651 weldment shown in Fig. 13 (b). The pore size influenced tensile strength, with coarser pores in the Al7075-T651 welded contributing to increased internal residual stress, requiring additional strength and ductility for rupture, and the same topographies were noticed in friction stir butt joint welding between the 6065 to 7075 alloys in reference [40]. The relationship between pore size and dimple features indicated a direct correlation with the strength and ductility of the joints; larger pores were associated with higher strength and ductility, while smaller pores related to lower strength and ductility. During the tensile test, the specimen undergoes ductile fracture, which results in the formation of small, round dimples that indicate the material experienced plastic deformation before failure on the advancing side of AA6061-T651 material. This occurs because, as the material stretches, voids form around second-phase particles, eventually joining and leading to failure and Similar structures were observed in reference [39], where the fracture surface exhibited dimples indicating ductile failure

The AA7075-T651 displays a blended-mode fracture, with both ductile and brittle features. Ductile areas of microstructure exhibit small dimples as shown in Fig. 13, caused by micro-void coalescence, indicating some plastic deformation. However, brittle regions, characterized by flat cleavage facets and secondary cracks, dominate, reflecting the alloy's high strength but lower ductility. The study notes some limitations. Specifically, the predictive models are based on idealized boundary conditions and assumptions that may not capture all real-world complexities,

such as microstructural heterogeneities or residual stress effects. The welding parameters explored represent a specific range optimized for the investigated configurations.

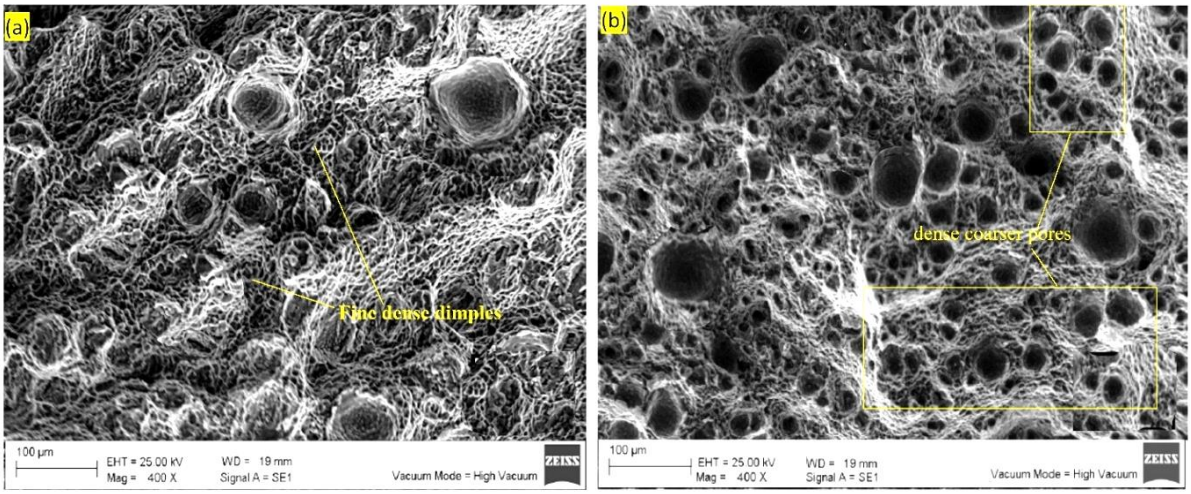

Fig. 13. SEM pictures of the FSW specimens' fracture surfaces (a) AA6061, (b) AA7075

4. Conclusions

This investigation employed the Taguchi method to determine optimal conditions for Multilayer Multipass friction stir welding of dissimilar AA6061-T651 and AA7075-T651 joints. The evaluation of experimental results was conducted utilizing the ANOVA tool. The impact of tool speed of rotation, welding speed, and tool tilt angle on the quality of joints in dissimilar AA6061-T651 and AA7075-T651 alloys was determined. From the analysis of this study, the following findings have been made:

- The ANOVA results show the significance of each parameter's contribution. Rotational speed seems to be the most crucial factor, accounting for 50.57% of the total contribution. In comparison, traverse speed and tool pin geometry contribute 13.98% and 35.10%, respectively, to the overall strength of the welded joint. This study offers a pathway for more efficient fabrication strategies in welding dissimilar aluminum alloys with various joint configurations. Whereas
- The optimum parameters for attaining the highest tensile strength of 202.65 MPa in friction stir welded joints include a speed of rotation of 1100 rpm, a welding speed of 20 mm/min, and the use of taper threadless pin tool geometry (T3). This can directly aid in the optimized design of welded joints, ensuring enhanced mechanical performance in structural applications.
- The fracture surfaces of AA6061-T651 and AA7075-T651 weldments in SEM analysis revealed that larger pores, particularly in the AA7075-T651 welded AA6061-T651, were associated with heightened internal residual stress, requiring additional strength and ductility for rupture, signifying a direct proportionality between pore size and the strength and ductility of the respective joints. This work supports additional reliable joining techniques for lighter, stronger, and more durable components.
- Compared to previous studies on dissimilar AA6061-AA7050 FSW joints [39, 40], the present investigation demonstrates superior mechanical strength and fracture resistance by enhancing interlayer bonding, eliminating internal defects, attributed to the multilayered multipass approach. The absence of voids and the presence of uniformly distributed dimples across fracture surfaces indicate improved material intermixing and structural integrity. These results reinforce the potential of the multipass FSW technique for producing high-integrity joints in high-strength aluminum alloys

4.1. Future Scope

- Extending the investigation to include other dissimilar alloy pairings and hybrid material systems. Ex: Aluminum-steel, Aluminum-magnesium
- Future studies could employ advanced microstructural and phase analysis (e.g., EBSD, TEM) to understand the metallurgical transformations occurring at the weld interface.
- The welded joints should undergo extensive mechanical testing to assess their durability under actual service conditions. This testing should include corrosion resistance, fatigue life, and fracture toughness.

Acknowledgment

We heartily express our gratitude to the National Institute of Technology Karnataka, Suratkal, for their assistance and resources, which contributed significantly to this study's success.

References

[1] Emamian SS, Awang M, Yusof F. Correction to: Advances in Manufacturing Engineering. 2021. Epub ahead of print 2021. https://doi.org/10.1007/978-981-15-5753-8
[2] Abolusoro OP, Akinlabi ET, Kailas S V. Impact of tool profile on mechanical behavior and material flow in friction stir welding of dissimilar aluminum alloys. Materialwissenschaft und Werkstofftechnik 2020; 51: 725-731. https://doi.org/10.1002/mawe.202000002
[3] Thomas WM. Friction Stir Butt Welding, International Patent Application No. PCT/GB92. GB Patent Application No 91259788.
[4] Thompson B, Doherty K, Niese C, et al. Friction stir welding of thick section aluminum for military vehicle applications. DTIC Online Document Access No ADA574537 Retrived from: http://oai dtic mil/oai/oai
[5] Imam M, Sun Y, Fujii H, et al. Friction stir welding of thick aluminium welds-challenges and perspectives. Friction Stir Welding and Processing IX 2017; 119-124. https://doi.org/10.1007/978-3-319-52383-5_13
[6] Kumar DA, Biswas P, Tikader S, et al. A study on friction stir welding of 12mm thick aluminum alloy plates. J Mar Sci Appl 2013; 12: 493-499. https://doi.org/10.1007/s11804-013-1221-y
[7] Liang Z, Wang X, Cai C, et al. Microstructure and mechanical properties of thick plate friction stir welds for 6082-T6 aluminum alloy. High Temperature Materials and Processes 2019; 38: 525-532. https://doi.org/10.1515/htmp-2018-0074
[8] Colegrove PA, Shercliff HR. CFD modelling of friction stir welding of thick plate 7449 aluminium alloy. Science and Technology of welding and joining 2006; 11: 429-441. https://doi.org/10.1179/174329306X107700
[9] Martin JP. Friction Stir Welding of Thick Section Aluminium Alloys-New Techniques. 2017, pp. 99-108. https://doi.org/10.1007/978-3-319-52383-5_11
[10] Lim YC, Sanderson S, Mahoney M, et al. Characterization of multilayered multipass friction stir weld on ASTM A572 G50 steel. Welding Journal; 93.
[11] Wang K, Khan HA, Li Z, et al. Micro friction stir welding of multilayer aluminum alloy sheets. Journal of Materials Processing Technology 2018; 260: 137-145. https://doi.org/10.1016/j.jmatprotec.2018.05.029
[12] Tariq M, Khan I, Hussain G, et al. Microstructure and micro-hardness analysis of friction stir welded bi-layered laminated aluminum sheets. International Journal of Lightweight Materials and Manufacture 2019; 2: 123-130. https://doi.org/10.1016/j.ijlmm.2019.04.010
[13] Sajed M, Hossein Seyedkashi SM. Multilayer friction stir plug welding: A novel solid-state method to repair cracks and voids in thick aluminum plates. CIRP Journal of Manufacturing Science and Technology 2020; 31: 467-477. https://doi.org/10.1016/j.cirpj.2020.07.009
[14] Gera D, Fu B, Suhuddin UFHR, et al. Microstructure, mechanical and functional properties of refill friction stir spot welds on multilayered aluminum foils for battery application. Journal of Materials Research and Technology 2021; 13: 2272-2286. https://doi.org/10.1016/j.jmrt.2021.06.017
[15] Taendl J, Nambu S, Inoue J, et al. Friction stir welding of multilayered steel. Science and Technology of Welding and Joining 2012; 17: 244-253. https://doi.org/10.1179/1362171812Y.0000000003
[16] Das A, Medhi T, Kapil S, et al. Multi-track multi-layer friction stir additive manufacturing of AA6061-T6 alloy. Progress in Additive Manufacturing. Epub ahead of print 2023. https://doi.org/10.1007/s40964-023-00485-w
[17] Chen L, Zhu L, Lu L, et al. The effect of heat treatment on the microstructure and electrochemical corrosion behavior of multilayer AA6061 alloy fabricated by additive friction stir deposition. Applied Surface Science 2024; 650: 159167. https://doi.org/10.1016/j.apsusc.2023.159167

[18] Hassan A, Awang M, Pedapati SR, et al. Experimental investigation on tool pin profile for defect-free multi-layered laminates using friction stir additive manufacturing. Results in Engineering 2023; 20: 101516. https://doi.org/10.1016/j.rineng.2023.101516
[19] Orłowska M, Brynk T, Hütter A, et al. Similar and dissimilar welds of ultrafine grained aluminium obtained by friction stir welding. Materials Science and Engineering: A 2020; 777: 139076. https://doi.org/10.1016/j.msea.2020.139076
[20] Yang Y, Paidar M, Mehrez S, et al. Enhancement of mechanical properties and wear of AA5083/316 stainless steel surface-composite developed through multi-pass friction stir processing (MPFSP). Archives of Civil and Mechanical Engineering 2022; 23: 13. https://doi.org/10.1007/s43452-022-00556-9
[21] Laska, A.; Szkodo, M.; Cavaliere, P.; Perrone A. Influence of the Tool Rotational Speed on Physical and Chemical Properties of Dissimilar Friction-Stir-Welded AA5083/AA6060 Joints. Metals 2022; 12: 1658. https://doi.org/10.3390/met12101658
[22] Laska, A.; Szkodo, M.; Koszelow, D.; Cavaliere P. Effect of Processing Parameters on Strength and Corrosion Resistance of Friction Stir-Welded AA6082. Metals 2022; 12: 192. https://doi.org/10.3390/met12020192
[23] Aleksandra Laska, Behzad Sadeghi, Behzad Sadeghian, Aboozar Taherizadeh, Marek Szkodo PC. Temperature Evolution, Material Flow, and Resulting Mechanical Properties as a Function of Tool Geometry during Friction Stir Welding of AA6082. J of Materi Eng and Perform 2023; 32: 10655-10668. https://doi.org/10.1007/s11665-023-08671-1
[24] Aleksandra Laska, Marek Szkodo, Pasquale Cavaliere, Dorota Moszczyńska JM. Analysis of Residual Stresses and Dislocation Density of AA6082 Butt Welds Produced by Friction Sir Welding. Metall Mater Trans A 2023; 54: 211-225. https://doi.org/10.1007/s11661-022-06862-4
[25] Cole EG, Fehrenbacher A, Duffie NA, et al. Weld temperature effects during friction stir welding of dissimilar aluminum alloys 6061-t6 and 7075-t6. The International Journal of Advanced Manufacturing Technology 2014; 71: 643-652. https://doi.org/10.1007/s00170-013-5485-9
[26] Seshu Kumar GS V, Anshuman K, Rajesh S, et al. Optimization of FSW process parameters for welding dissimilar 6061 and 7075 Al alloys using Taguchi design approach. International Journal of Nonlinear Analysis and Applications 2022; 13: 1011-1022. https://doi.org/10.1007/s12008-022-00913-1
[27] Ghiasvand A, Noori SM, Suksatan W, et al. Effect of Tool Positioning Factors on the Strength of Dissimilar Friction Stir Welded Joints of AA7075-T6 and AA6061-T6. Materials; 15. Epub ahead of print 2022. https://doi.org/10.3390/ma15072463
[28] Ghiasvand A, Suksatan W, Tomków J, et al. Investigation of the Effects of Tool Positioning Factors on Peak Temperature in Dissimilar Friction Stir Welding of AA6061-T6 and AA7075-T6 Aluminum Alloys. Materials; 15. Epub ahead of print 2022. https://doi.org/10.3390/ma15030702
[29] Chen Y, Cai Z, Ding H, et al. The Evolution of the Nugget Zone for Dissimilar AA6061/AA7075 Joints Fabricated via Multiple-Pass Friction Stir Welding. Metals; 11. Epub ahead of print 2021. https://doi.org/10.3390/met11101506
[30] Parasuraman P, Sonar T, Rajakumar S. Microstructure, tensile properties and fracture toughness of friction stir welded AA7075-T651 aluminium alloy joints. 2022; 64: 1843-1850. https://doi.org/10.1515/mt-2022-0212
[31] Lim YC, Sanderson S, Mahoney M, et al. Mechanical properties and microstructural characterization of a multilayered multipass friction stir weld in steel. Friction Stir Welding and Processing VII 2016; 81-90. https://doi.org/10.1007/978-3-319-48108-1_9
[32] Bahemmat P, Haghpanahi M, Besharati MK, et al. Study on mechanical, micro-, and macrostructural characteristics of dissimilar friction stir welding of AA6061-T6 and AA7075-T6. Proceedings of the Institution of Mechanical Engineers, Part B: Journal of Engineering Manufacture 2010; 224: 1854-1864. https://doi.org/10.1243/09544054JEM1959
[33] Nandan R, DebRoy T, Bhadeshia H. Recent advances in friction-stir welding-process, weldment structure and properties. Progress in materials science 2008; 53: 980-1023. https://doi.org/10.1016/j.pmatsci.2008.05.001
[34] Bhardwaj N, Narayanan RG, Dixit US, et al. Recent developments in friction stir welding and resulting industrial practices. Advances in Materials and Processing Technologies 2019; 5: 461-496. https://doi.org/10.1080/2374068X.2019.1631065
[35] Safeen W, Hussain S, Wasim A, et al. Predicting the tensile strength, impact toughness, and hardness of friction stir-welded AA6061-T6 using response surface methodology. The International Journal of Advanced Manufacturing Technology 2016; 87: 1765-1781. https://doi.org/10.1007/s00170-016-8565-9
[36] Standard Test Methods for Tension Testing of Metallic Materials. ASTM E8-E8M. Mar 05, 2024.

[37] Krishna Reddy G. V, Yashwant Chapke, Hareesha G SD. Effects of addition of graphite on the tribological behaviour of Al7075-SiC Hybrid Composites using Design of Experiments. Journal of Bio- and Tribo-Corrosion; 10. Epub ahead of print 2024. https://doi.org/10.1007/s40735-024-00880-y
[38] Lingaraju SV, Gururaj Hatti, Mahesh R. Jadhav, Mukund S. Dhuttargaon SD. Investigation on Tribological Behavior of Al7075-TiC/Graphene Nano-composite Using Taguchi Method. J Bio Tribo Corros; 10. Epub ahead of print 2024. https://doi.org/10.1007/s40735-024-00908-3
[39] Guo JF, Chen HC, Sun CN, et al. Friction stir welding of dissimilar materials between AA6061 and AA7075 Al alloys effects of process parameters. Materials & Design (1980-2015) 2014; 56: 185-192. https://doi.org/10.1016/j.matdes.2013.10.082
[40] Rodriguez RI, Jordon JB, Allison PG, et al. Microstructure and mechanical properties of dissimilar friction stir welding of 6061-to-7050 aluminum alloys. Materials and Design 2015; 83: 60-65. https://doi.org/10.1016/j.matdes.2015.05.074
[41] Korgal A, Upadhyaya S, T A. Grain refinement of aluminium 4032 alloy with the impact of vibration using Taguchi technique and analysis of variance (ANOVA). Materials Today: Proceedings 2022; 54: 507-512. https://doi.org/10.1016/j.matpr.2021.11.504
[42] Hareesha Guddhur, Chikkanna Naganna SD. Taguchi's method of optimization of fracture toughness parameters of Al-SiCp composite using compact tension specimens.
[43] Das U, Toppo V. Effect of tool rotational speed on temperature and impact strength of friction stir welded joint of two dissimilar aluminum alloys. Materials Today: Proceedings 2018; 5: 6170-6175. https://doi.org/10.1016/j.matpr.2017.12.223
[44] Lim Y. C, Sanderson S., Mahoney M., et al. Fabrication of thick multilayered steel structure using A516 Grade 70 by multipass friction stir welding†. Science and Technology of Welding and Joining 2016; 21: 564-569. https://doi.org/10.1080/13621718.2016.1142138